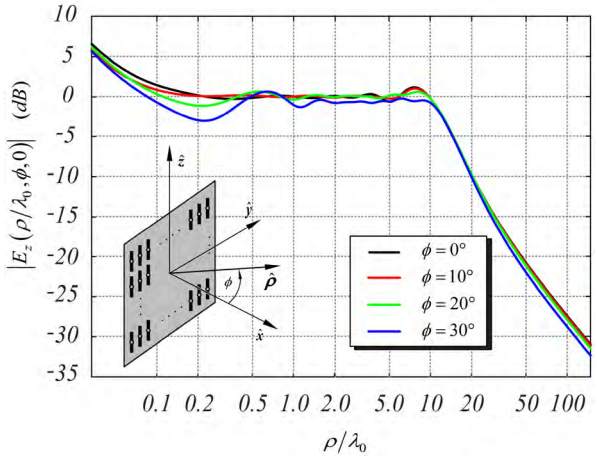

FIGURE 8. Electric field magnitude ($z-$component) for the truncated Bessel beam along the $\rho-$axis for different $\phi-$ angles. Noteworthy is the spatial behavior of the field that, beyond a distance of about $10\lambda_0$, presents a rapid falloff before decaying to the spherical wave propagation regime that occurs at about $30\lambda_0$ from the array surface.

at larger pointing angles. Finally, as observed for broadside beams [10], the starting of the transition towards the spherical propagation regime occurs at a distance which roughly coincides with the vertex of the geometric optics (*GO*) shadow boundary of the Bessel beam field.

C. SYNTHESIS OF OAM BESSEL BEAMS

A second example, consisting of the synthesis of Bessel beams carrying orbital angular momentum (OAM), is presented to show the suitability of the synthesis approach based on the target electric field only in synthesizing accurately such complex magnitude and phase distributions. OAM Bessel beams may be particularly advantageous in real applications due to their interesting "self-healing" properties, which may limit waveform degradation caused by obstacles in free-space optical and RF communication systems [11]–[13] since, under certain conditions, they have been shown to be more robust than non-Bessel OAM beams [11].

The synthesis of OAM beams has been performed using the following target electric field

$$\boldsymbol{E}_t^{(Target)}(\rho,\phi) = J_n\left[\beta_\rho\,\rho\right] circ\left[\frac{\beta_\rho\,\rho}{\xi_{nm}}\right] e^{jn\phi}\hat{\boldsymbol{z}} \qquad (10)$$

where $\beta_\rho = 0.3\,\beta_0$, $circ\,[\cdot]$ is the circle function, while ξ_{nm} is the $m-th$ zero of the $n-th$ order Bessel function.

Magnitude and phase plots for the synthesized OAM Bessel beams at $x_s = \lambda_0$ up to the third order ($m = 3$ for the first two beams, and $m = 2$ for the third one) are reported in Fig. 9. The respective *NMSE* figures ($-25.4dB$, $-23.6dB$, and $-25.7dB$) indicate excellent magnitude and phase

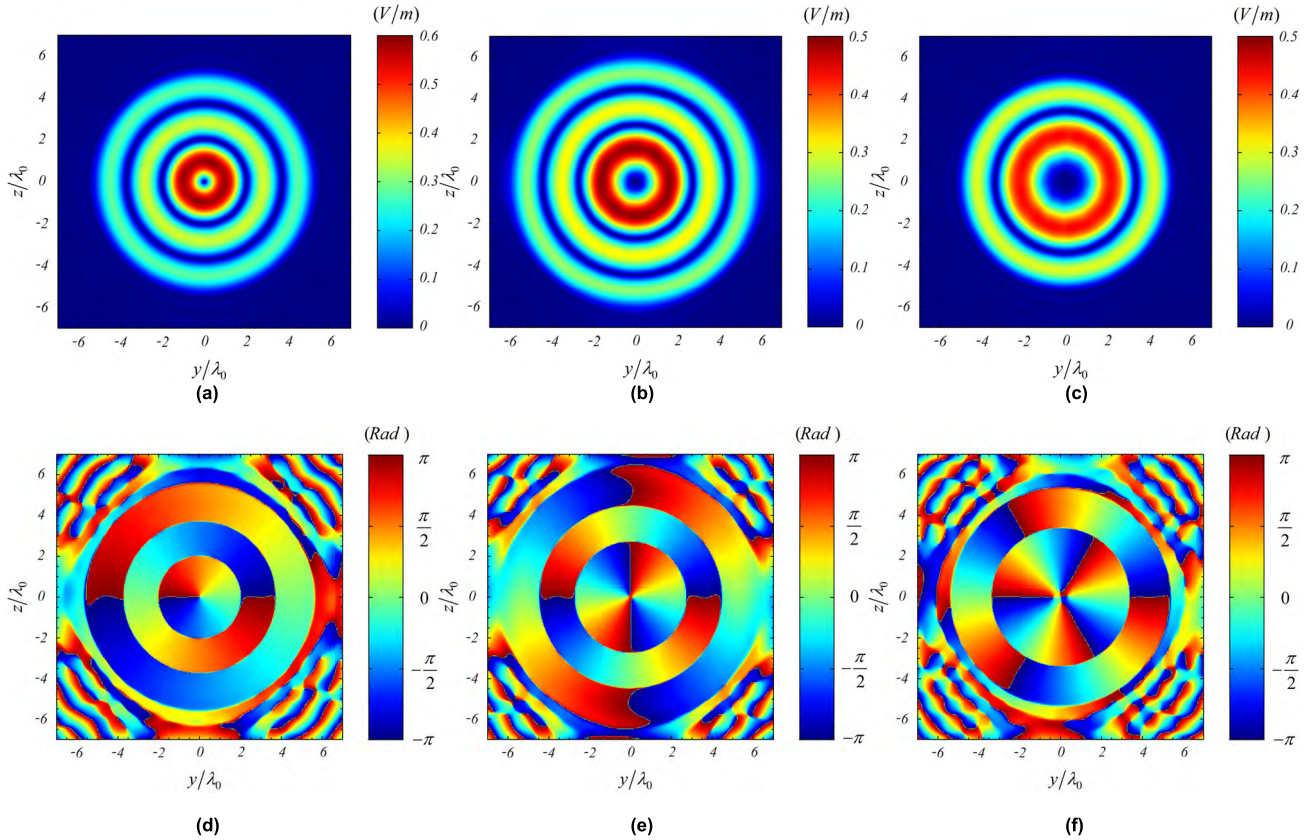

FIGURE 9. Spatial distribution of the magnitude (first-row) and phase (second-row) of the electric field (z-component) of OAM Bessel beams on the synthesis surface at $x_s = \lambda_0$: (a) and (d) first-order, (b) and (e) second-order, and (c) and (f) third-order. An excellent accuracy in the synthesis of the OAM Bessel target field (magnitude and phase) can be observed in the figure.

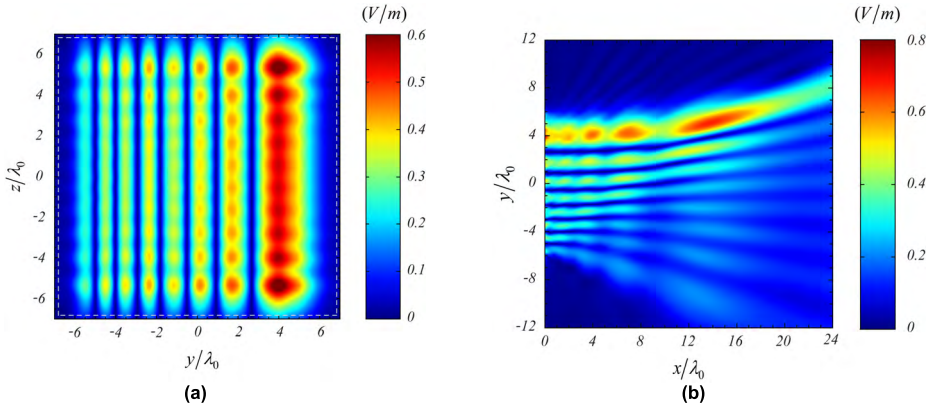

FIGURE 10. Spatial distribution of the electric field (z-component) of the Airy beam computed in the synthesis plane at $x_s = \lambda_0$ (a), and in the xy-plane at z = 0 (b). The peaks appearing in the field map in the yz-plane are related to the maximums of the Airy function even if they suffer from the presence of diffractive processes taking place along the array contour, while the typical parabolic profile of the electric field is observed in the xy-plane. The dashed line outlines the reflector footprint.

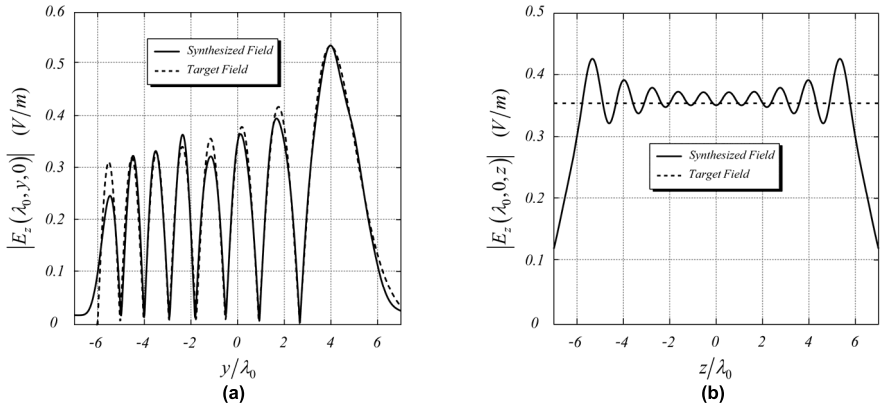

FIGURE 11. Electric field magnitude (z-component) excited at $x_s = \lambda_0$ from the array aperture, for the truncated Airy function with $x_0 = \lambda_0$ computed along the y-direction at z = 0 (a), and along the z-direction at y = 0 (b). A good agreement with the target field can be observed.

accuracy, as required to limit crosstalk between different orbital mode channels [11].

D. SYNTHESIS OF AIRY BEAMS

A further example consists in the synthesis of an Airy beam, a particular field distribution that captured the attention of the optics community due to its diffraction-resistant characteristics enabling a broad range of applications, such as light trajectory control, wavefront self-healing, optical micromanipulation, etc. [14], [16]. A ray-optics analysis of Airy beams reveals that they are characterized by the field propagation occurring on parabolic paths along which most of the RF energy is concentrated [16]. This important feature makes Airy beams useful in micromanipulation of particles [16] or in upcoming applications involving through-the-wall imaging where obstacles may be stationed between the RF source and the electromagnetic target.

The $2-D$ maps of the electric field $z-$component synthesized at $x_s = \lambda_0$ upon assigning the following Airy target field

$$\boldsymbol{E}_t^{(Target)}(y,z) = \begin{cases} Ai\left[\dfrac{y-y_0}{\lambda_0}\right]\hat{z}\ \forall y \in [-6\lambda_0, 7\lambda_0], & z \in [-7\lambda_0, 7\lambda_0] \\ 0, & \text{otherwise} \end{cases} \tag{11}$$

with $y_0 = 5\lambda_0$, are shown in Fig. 10, while the related amplitude profiles along the $y-$direction at $z = 0$, and along the $z-$direction at $y = 0$ are reported in Figs. 11a and 11b, respectively. As shown in Fig. 10, the main beam as well as a few secondary beams follow a parabolic profile along the caustic, while the remaining beams feature an opposite bend in their propagation path due to diffraction at the array truncation. In addition, the diffractive effects occurring along the array contour cause field magnitude fluctuations, clearly visible in Fig. 11. Although the field spatial behavior is in good agreement with the target, a higher error ($NMSE = -11.5dB$) is observed in comparison with the Bessel beam synthesis, due to the larger spatial variations of the Airy target field. This error may be reduced using larger arrays.

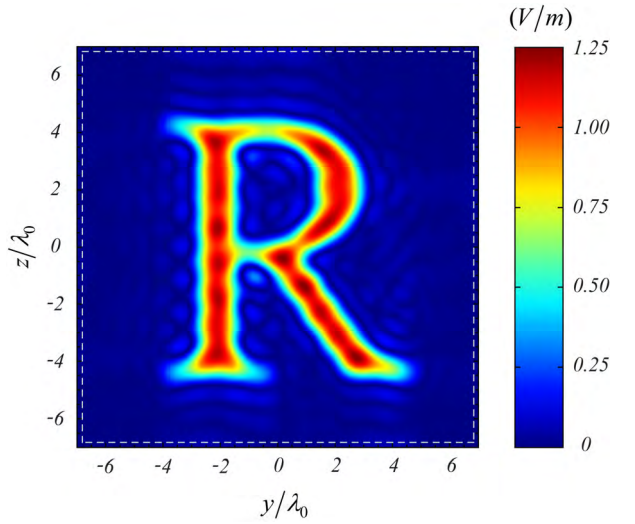

FIGURE 12. Spatial distribution of the electric field (z-component) of the R-shaped beam synthesized on closed surface at $x_s = \lambda_0$. An excellent agreement with the target field is observed. The white dashed line outlines the 21 × 21 element array reflector footprint.

E. SYNTHESIS OF STRONGLY ASYMMETRIC FIELDS

The last example features the synthesis of a strongly asymmetric near field beam, consisting of the Times New Roman character "R". In Fig. 12 the $2-D$ map, computed at $x_s = \lambda_0$, of the $z-$polarized electric field having unit amplitude in the domain corresponding to the character "R" is reported to show the flexibility of the $E-$field synthesis approach applied to arbitrary target fields. As it can be observed also in this case the agreement with the target field is excellent ($NMSE = -8.6dB$).

IV. CONCLUSIONS

A field synthesis procedure, based on the eigenfields of the radiation matrix of a multiport radiating structure, was employed to synthesize near fields having complex spatial distributions. The numerical results showed that near-field synthesis performed by means of target electric and magnetic fields exhibits numerical accuracy similar to those based on the target electric field alone. In addition, it has been observed that field synthesis performed on open surfaces feature a higher accuracy within the target area but much smaller accuracy outside, whereas synthesis based on closed target field surfaces are more burdensome numerically but extremely more accurate outside the target area, particularly at large distance from the array surface. Nevertheless, the two approaches provide similar numerical accuracy when the synthesis surfaces are close to the array, or when modal filtering is suitably applied to remove eigenfields featuring low efficiency. In fact, while for the synthesis on closed surfaces the modal filtering has a very limited impact, it assumes a key role to synthesize good quality field distributions on open surfaces located far from the array plane. This finding may be exploited for reducing the computational burden especially in real-time tracking applications. Finally, propagation characteristics of diffraction-resistant Bessel, OAM Bessel and Airy beams in their actual finite-energy implementation, when excited by antenna arrays of finite dimensions, have been investigated. Bessel beams were found to decay towards the spherical wave propagation regime at about the same distance for different beam tilt angles, while synthesized Airy beams propagate along parabolic caustics except for far secondary beams placed near the array boundary due to diffractive effects occurring at the array truncation. Based on the foregoing analysis, the proposed near-field technique appears to be suitable for deriving array excitation profiles that may synthesize accurately uncommonly complex near field distributions.

APPENDIX

The target fields employed to synthesize Bessel beams are given by

$$E_y(x,y,z) = 0 \tag{A1}$$

$$E_z(x,y,z) = E_0 J_0\left(\beta_\rho \sqrt{y^2+z^2}\right) circ\left[\frac{\beta_\rho \sqrt{y^2+z^2}}{\xi_{04}}\right] e^{-jx\sqrt{\beta_0^2-\beta_\rho^2}} \tag{A2}$$

$$H_y(x,y,z) = -\frac{E_0}{\eta_0}\frac{\beta_\rho^2}{\gamma\,\beta_0}\left[\left(\frac{\beta_0^2}{\beta_\rho^2}-\frac{y^2}{y^2+z^2}\right) J_0\left(\beta_\rho\sqrt{y^2+z^2}\right) + \frac{1}{\beta_\rho\sqrt{y^2+z^2}}\,\frac{y^2-z^2}{y^2+z^2}\,J_1\left(\beta_\rho\sqrt{y^2+z^2}\right)\right] \cdot circ\left[\frac{\beta_\rho\sqrt{y^2+z^2}}{\xi_{04}}\right] e^{-jx\sqrt{\beta_0^2-\beta_\rho^2}} \tag{A3}$$

$$H_z(x,y,z) = \frac{E_0}{\eta_0}\frac{\beta_\rho^2}{\gamma\,\beta_0}\,\frac{yz}{y^2+z^2}\left[J_0\left(\beta_\rho\sqrt{y^2+z^2}\right) - \frac{2}{\beta_\rho\sqrt{y^2+z^2}}\,J_1\left(\beta_\rho\sqrt{y^2+z^2}\right)\right] \cdot circ\left[\frac{\beta_\rho\sqrt{y^2+z^2}}{\xi_{04}}\right] e^{-jx\sqrt{\beta_0^2-\beta_\rho^2}} \tag{A4}$$

with

$$\gamma = \sqrt{\beta_0^2-\beta_\rho^2}, \tag{A5}$$

where E_0 defines the maximum value of the electric field amplitude, $circ\,[\cdot]$ is the circle function and $\xi_{04} \simeq 11.7915$ is the fourth zero of the zeroth order Bessel function, η_0 is the free-space characteristic impedance, while β_0 and β_ρ are the free-space and the radial wavenumbers, respectively. The target field components useful for the synthesis of tilted Bessel beams, rotated by an angle ϕ in the xy plane, can be evaluated using the usual transformation formulas between orthogonal coordinate systems.

ACKNOWLEDGMENT

The authors are grateful to Dr. G. (Goga) Bit-Babik at the Motorola Solutions Chief Technology Office for his expert

assistance in MoM simulation analysis and M. Mazzetta of the University of Rome "La Sapienza" for IT technical support.

REFERENCES

[1] F. Tofigh, J. Nourinia, M. Azarmanesh, and K. M. Khazaei, "Near-field focused array microstrip planar antenna for medical applications," *IEEE Antennas Wireless Propag. Lett.*, vol. 13, pp. 915–954, 2014.
[2] X. He, W. Geyi, and S. Wang, "Optimal design of focused arrays for microwave-induced hyperthermia," *IET Microw., Antennas Propag.*, vol. 9, no. 14, pp. 1605–1611, Nov. 2015.
[3] N. Shinohara, "Power without wires," *IEEE Microw. Mag.*, vol. 12, no. 7, pp. S64–S73, Dec. 2011.
[4] G. Oliveri, L. Poli, and A. Massa, "Maximum efficiency beam synthesis of radiating planar arrays for wireless power transmission," *IEEE Trans. Antennas Propag.*, vol. 61, no. 5, pp. 2490–2499, May 2013.
[5] H. Sun and W. Geyi, "Optimum design of wireless power transmission systems in unknown electromagnetic environments," *IEEE Access*, vol. 5, pp. 20198–20206, Oct. 2017.
[6] K. E. Browne, R. J. Burkholder, and J. L. Volakis, "Through-wall opportunistic sensing system utilizing a low-cost flat-panel array," *IEEE Trans. Antennas Propag.*, vol. 59, no. 3, pp. 859–868, Mar. 2011.
[7] G. Gennarelli, G. Vivone, P. Braca, F. Soldovieri, and M. G. Amin, "Multiple extended target tracking for through-wall radars," *IEEE Trans. Geosci. Remote Sens.*, vol. 53, no. 12, pp. 6482–6494, Dec. 2015.
[8] P. Lemaitre-Auger, S. Abielmona, and C. Caloz, "Generation of Bessel beams by two-dimensional antenna arrays using sub-sampled distributions," *IEEE Trans. Antennas Propag.*, vol. 61, no. 4, pp. 1838–1849, Apr. 2013.
[9] D. McGloin, V. Garcés-Chávez, and K. Dholakia, "Interfering Bessel beams for optical micromanipulation," *Opt. Lett.*, vol. 28, no. 8, pp. 657–659, Apr. 2003.
[10] D. McGloin and K. Dholakia, "Bessel beams: Diffraction in a new light," *Contemp. Phys.*, vol. 46, no. 1, pp. 15–28, Jan./Feb. 2005.
[11] N. Ahmed *et al.*, "Mode-division-multiplexing of multiple Bessel-Gaussian beams carrying orbital-angular-momentum for obstruction-tolerant free-space optical and millimetre-wave communication links," *Sci. Rep.*, vol. 6, Mar. 2016, Art. no. 22082.
[12] X. Chu, Q. Sun, J. Wang, P. Lü, W. Xie, and X. Xu, "Generating a Bessel-Gaussian beam for the application in optical engineering," *Sci. Rep.*, vol. 5, Dec. 2015, Art. no. 18665.
[13] M. Veysi, C. Guclu, F. Capolino, and Y. Rahmat-Samii, "Revisiting orbital angular momentum beams: Fundamentals, reflectarray generation, and novel antenna applications," *IEEE Antennas Propag. Mag.*, vol. 60, no. 2, pp. 68–81, Apr. 2018.
[14] I. D. Chremmos, G. Fikioris, and N. K. Efremidis, "Accelerating and abruptly-autofocusing beam waves in the fresnel zone of antenna arrays," *IEEE Trans. Antennas Propag.*, vol. 61, no. 10, pp. 5048–5056, Oct. 2013.
[15] R. Cicchetti, A. Faraone, and O. Testa, "Energy-based representation of multiport circuits and antennas suitable for near- and far-field syntheses," *IEEE Trans. Antennas Propag.*, vol. 67, no. 1, pp. 85–98, Jan. 2019.
[16] J. Baumgartl, M. Mazilu, and K. Dholakia, "Optically mediated particle clearing using Airy wavepackets," *Nature Photon.*, vol. 2, pp. 675–678, Nov. 2008.
[17] W. Wen and X. Chu, "Quantitative comparison of self-healing ability between Bessel–Gaussian beam and Airy beam," *Ann. Phys.*, vol. 360, pp. 549–555, Sep. 2015.
[18] R. Kadlimatti and P. V. Parimi, "Millimeter-wave nondiffracting circular Airy OAM beams," *IEEE Trans. Antennas Propag.*, vol. 67, no. 1, pp. 260–269, Jan. 2019.
[19] K. Liu *et al.*, "Generation of OAM beams using phased array in the microwave band," *IEEE Trans. Antennas Propag.*, vol. 64, no. 9, pp. 3850–3857, Sep. 2016.
[20] Ö. A. Çivi, P. H. Pathak, H.-T. Chou, and P. Nepa, "A hybrid uniform geometrical theory of diffraction–moment method for efficient analysis of electromagnetic radiation/scattering from large finite planar arrays," *Radio Sci.*, vol. 35, no. 2, pp. 607–620, Mar./Apr. 2000.
[21] P. Bernardi, R. Cicchetti, and O. Testa, "An accurate UTD model for the analysis of complex indoor radio environments in microwave WLAN systems," *IEEE Trans. Antennas Propag.*, vol. 52, no. 6, pp. 1509–1520, Jun. 2004.

RENATO CICCHETTI (S'83–M'83–SM'01) was born in Rieti, Italy, in 1957. He received the Laurea degree *(summa cum laude)* in electronics engineering from the Sapienza University of Rome, Rome, Italy, in 1983. From 1983 to 1986, he was an Antenna Designer with Selenia Spazio S.p.A. (now Thales Alenia Space S.p.A.), Rome, where he was involved in the studies on theoretical and practical aspects of antennas for space application and scattering problems. From 1986 to 1994, he was a Researcher, and from 1994 to 1998, he was an Assistant Professor with the Department of Electronics Engineering, Sapienza University of Rome, where he is currently a Full Professor. He was a Visiting Professor with the Motorola Florida Corporate Electromagnetics Research Laboratory, Fort Lauderdale, FL, USA, in 1998, 2002, and 2006, where he was involved in antennas for cellular and wireless communications. Since 2012, he has been the Lead Editor of the annual special issue on Wideband, Multiband, Tunable, and Smart Antenna Systems For Mobile UWB Wireless Applications for the *International Journal of Antennas and Propagation*, while he is currently one of the coordinators of the research project ultra-wideband virtual imaging extra wall for high-penetration, high-quality imagery of enclosed structures (U-VIEW) supported by the Italian Ministry of Education, University and Research (MIUR). His current research interests include electromagnetic field theory, asymptotic techniques, electromagnetic compatibility, wireless communications, microwave and millimeter-wave integrated circuits, and antennas. He is a Member of the Italian Electromagnetic Society (*SIEm*), and his results listed in Marquis *Who's Who in the World* and *Who's Who in Science and Engineering*.

ANTONIO FARAONE (M'97–SM'05) was born in Rome, Italy, in 1966. He received the Ph.D. degree in applied electromagnetics from the Sapienza University of Rome Sapienza, in 1997, then he joined the Motorola (now Motorola Solutions, Inc.) Corporate Electromagnetic Energy (EME) Research Laboratory, Fort Lauderdale, FL, USA, where he is currently involved in mobile antenna technology and RF dosimetry research, and RF exposure safety and product compliance standards development. He currently oversees RF exposure compliance matters as the Chief EME Scientist with Motorola Solutions, where he is a Scientific Advisory Board Associates (SABA) Member, Master Innovator, and Dan Noble Fellow. He holds 37 patents, mostly in antenna technologies. He has coauthored 36 refereed journal publications, and he continues to be actively involved in the IEEE and IEC standards related to safe EME exposure. He currently serves as the Chair of the Mobile & Wireless Forum, an international industry association supporting research into RF health and safety and promoting device integrity and accessibility.

ORLANDINO TESTA was born Minturno, Italy, in 1972. He received the Laurea degree *(cum laude)* in electronic engineering and the Ph.D. degree from the Sapienza University of Rome, Rome, Italy, in 1997 and 2003, respectively. Since 2001, he has been the High School Teacher with I.T.I.S. G. Armellini, Institute of Rome, where he is involved in teaching electronics and telecommunications. He is also currently collaborating with the Department of Electronic Engineering, Sapienza University of Rome. He is currently studying high-frequency models for the analysis of radio coverage in indoor environments and tunnels with a particular attention to EMC/EMI problems. His main research interests include propagation and the radiation of electromagnetic fields, electromagnetic compatibility, microwave and millimeter-wave integrated circuits, and antennas.